Omnidirectional ADE Antennas with Shaped Main Reflector Described by Local Conic Sections Sequentially Concatenated

Rafael A. Penchel[1], José R. Bergmann[2]
CETUC - PUC-Rio
Rio de Janeiro, RJ 22453-130
rapenchel@cetuc.puc-rio.com[1],bergmann@cetuc.puc-rio.br[2]

Fernando J. S. Moreira
Dept. Electronics Engineering - UFMG
Belo Horizonte, MG 31270-901
fernandomoreira@ufmg.br

Abstract—**This work presents an extension of the formulation for the synthesis of dual-reflector antennas with omnidirectional coverage and arbitrary radiation pattern in elevation plane. The body-of-revolution subreflector is generated by a single conic section while the shaped main reflector is generated by a series of local conic sections sequentially consecutively concatenated. As case studies, four representative axis-displaced ellipse (ADE) configurations are synthesized to provide a sectoral coverage in the elevation plane. Two different ray structures are considered: with a real or a virtual main reflector caustic. The GO shaping results are validated using method-of-moments analysis.**

Keywords—**Geometrical optics, reflector antenna, conic sections, omnidirectional radiation pattern**.

I. INTRODUCTION

Some studies have dealt with the shaping of dual-reflector antennas for omnidirectional coverage by solving an ordinary differential equation derived from Geometrical Optics (GO) principles [1]–[3]. A different shaping technique based on the combination of local conic sections was presented for the shaping of Cassegrain and Gregorian antennas [4]. The formulation was improved and extended for the treatment of general circularly symmetric dual-reflector arrangements [5]. The shaping procedure was finally extended to the shaping of omnidirectional dual-reflector configurations providing uniform phase distribution at the main-reflector cylindrical aperture [6]. Recently, the concepts presented in [4]–[6] have been applied to the design of omnidirectional axis-displaced Cassegrain (OADC) dual-reflector antennas where only the main reflector was shaped to provide the desired radiation pattern in the elevation plane [7]. The present work proposes an extension of the OADC formulation presented in [7] to the main-reflector shaping of omnidirectional axis-displaced ellipse (OADE) dual-reflector antennas. **T**wo different ray structures are considered in the present investigation: one with a real and another with a virtual main-reflector caustic in the elevation plane. To illustrate the synthesis procedure, designs with specifications similar to those in [7] are presented.

II. MAIN-REFLECTOR SHAPING TECHNIQUE

In the present shaping method, the axis-symmetric (both sub and main reflectors are bodies of revolution) subreflector is generated by a single conic section, while the main reflector is generated by a combination of local conic sections, sequentially concatenated to each other. A procedure for the definition of the subreflector conic generatrix is not discussed here but it can be determined with the help of [8]. The subreflector conic section has two focci: one located at the origin (O), where the feed phase center is placed, and another at P, which defines the subreflector real annular caustic after the generatrix is rotated about the z-axis (see Fig. 1). As the subreflector conic section is known, the relation between the feed-ray direction (θ_F) and the direction of the ray reflected by the subreflector (θ_S) is also known from Snell's Law.

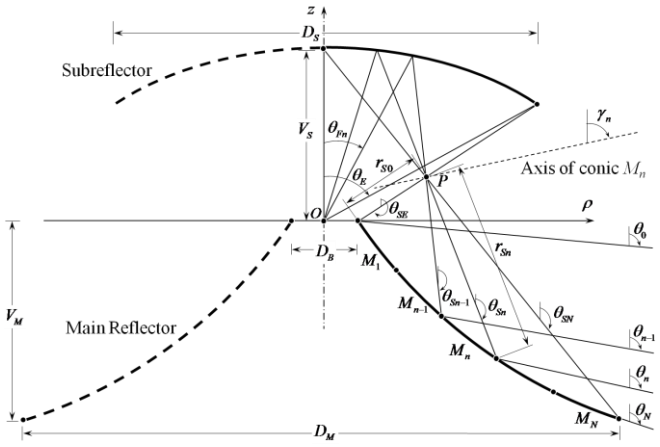

Fig. 1 - Conic sections representing the generatrix shaped main reflector

Note that, due to the presence of a real annular caustic P between the reflectors, the feed illumination toward the main reflector is inverted and, consequently, the ray structure is different from that of the OADC configuration investigated in [7]. So, rays departing from the dual-reflector focus O with directions $\theta_F = 0$ and $\theta_F = \theta_E$ reach the main-reflector outer and inner rims, respectively (see Fig. 1).

The main reflector is generated by local conic sections M_n (n = 1,…, N) sequentially concatenated, all of them with one of their focci coinciding with P. The axis of M_n passes through P and makes an angle γ_n with the z-direction (see Fig. 1). In order to uniquely determine the main-reflector conic sections M_n, three parameters must be determined for each M_n: the inter-focal

distance ($2c_n$), the eccentricity (e_n), and the angle γ_n of the conic axis, with the help of the following parameters [9]:

$$a_n = c_n\left(e_n - 1/e_n\right) \tag{1}$$

$$b_n = e_n \sin\gamma_n \tag{2}$$

$$d_n = e_n \cos\gamma_n - 1 \tag{3}$$

Three equations are needed to obtain the parameters a_n, b_n, and d_n for each step n of the iterative process. From the polar equation of M_n, the distance r_S from P to M_n is given by:

$$r_S = \frac{a_n}{b_n \sin\theta_S + (1+d_n)\cos\theta_S - 1}, \quad \text{for } \theta_{Sn-1} \le \theta_S \le \theta_{Sn} \tag{4}$$

As θ_{Sn-1} and r_{Sn-1} are known from the previous step (n–1), from (4) one obtains:

$$r_{Sn-1} = \frac{a_n}{b_n \sin\theta_{Sn-1} + (1+d_n)\cos\theta_{Sn-1} - 1} \tag{5}$$

From the polar equation of M_n one also obtains that

$$b_n\left[\cot\left(\frac{\theta}{2}\right) + \cot\left(\frac{\theta_S}{2}\right)\right] + d_n\left[\cot\left(\frac{\theta}{2}\right)\cot\left(\frac{\theta_S}{2}\right) - 1\right] = 2, \tag{6}$$

for $\theta_{Sn-1} \le \theta_S \le \theta_{Sn}$ and $\theta_{n-1} \le \theta \le \theta_n$, where θ is the direction of the ray reflected by the main reflector (see Fig. 1). As θ_{Sn-1} and θ_{n-1} are both known from the previous step, from (6) one obtains:

$$b_n\left[\cot\left(\frac{\theta_{n-1}}{2}\right) + \cot\left(\frac{\theta_{Sn-1}}{2}\right)\right] + d_n\left[\cot\left(\frac{\theta_{n-1}}{2}\right)\cot\left(\frac{\theta_{Sn-1}}{2}\right) - 1\right] = 2 \tag{7}$$

The conservation of energy along the tube of rays departing from O toward the main-reflector far-field region is finally imposed in an integral form:

$$\int_{\theta_{Fn}}^{\theta_E} G_F(\theta_F)\sin\theta_F \, \mathrm{d}\theta_F = N_F \int_{\theta_0}^{\theta_n} G_A(\theta)\sin\theta \, \mathrm{d}\theta \tag{8}$$

where $G_F(\theta_F)$ and $G_A(\theta)$ are the circularly-symmetric radiation patterns of the feed and the antenna, respectively, θ_0 is the prescribed direction of the ray reflected by the main reflector corresponding to the feed ray ($\theta_F = \theta_E$), and N_F is a normalization constant give by

$$N_F = \int_0^{\theta_E} G_F(\theta_F)\sin\theta_F \, \mathrm{d}\theta_F \Big/ \int_{\theta_0}^{\theta_N} G_A(\theta)\sin\theta \, \mathrm{d}\theta \tag{9}$$

where θ_0 and θ_N are the far field angular limits, under GO principles. If $\theta_0 > \theta_N$ the structure of rays corresponds to a main reflector with real caustic in the elevation (vertical) plane. If $\theta_N > \theta_0$, then the main-reflector caustic is virtual, as illustrated in Fig. 1. Once θ_n is numerically determined from (8), the third shaping equation is obtained from (6):

$$b_n\left[\cot\left(\frac{\theta_n}{2}\right) + \cot\left(\frac{\theta_{Sn}}{2}\right)\right] + d_n\left[\cot\left(\frac{\theta_n}{2}\right)\cot\left(\frac{\theta_{Sn}}{2}\right) - 1\right] = 2 \tag{10}$$

From (5), (7), and (9) a set of three linear equations are established to determine a_n, b_n, d_n, and, with the help of (1)-(3), $2c_n$, e_n, γ_n.

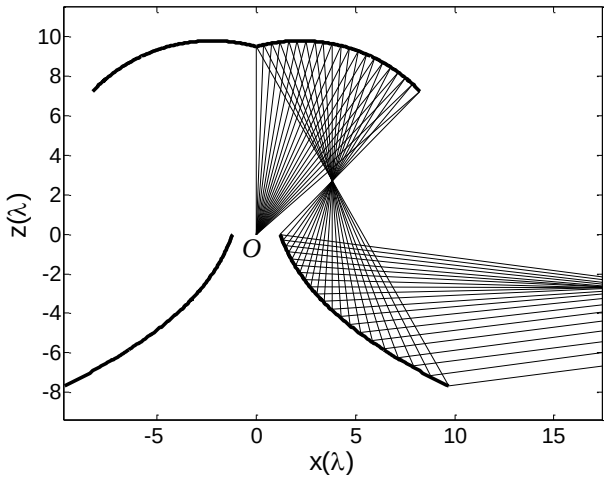

Fig. 2 – Generatrices of a shaped OADE dual-reflector antenna (Case A.I) with a real main-reflector caustic in the elevation plane.

For the OADE antenna, the iterative process starts at $n = 0$, with $\theta_{F0} = \theta_E$ (θ_{SE} is obtained from θ_E with the help of the subreflector conic equation), $\theta = \theta_0$, and r_{S0} given by the location of the subreflector caustic P and by the desired diameter D_B of the main-reflector central opening (see Fig. 1).

III. CASE STUDIES

To illustrate the shaping technique described in the Sect. II, four case studies are presented. The first two examples are designed to provide a sectoral coverage in the elevation plane over ±7.5° with respect to the horizon with real (Case A.I) or virtual (Case A.II) main-reflector caustic in the elevation plane. The last two cases provide sectoral coverage over ±15° with respect to the horizon with real (Case B.I) or virtual (Case B.II) main-reflector caustic. The feed is assumed to be a TEM coaxial horn which the function that describes the radiation pattern in the far-field region is given by [2]:

$$G_F\left(\theta_F\right) = G_{0F}\left[\frac{J_0\left(kr_i \sin\theta_F\right) - J_0\left(kr_e \sin\theta_F\right)}{\sin\theta_F}\right]^2 \tag{11}$$

where G_{0F} is a normalization factor. The internal and external aperture radii are $r_i = 0.45\lambda$ and $r_e = 0.90\lambda$, respectively. The objective function that describes the constant sectoral radiation pattern of the dual-reflector antenna in the elevation plane is given by [7]:

$$G_A\left(\theta\right) = \frac{1}{2\pi}\left|\frac{1}{\cos\theta_1 - \cos\theta_2}\right| \tag{12}$$

which has been normalized for unit radiated power.

A. *OADE Configuration for Sectoral Coverage over ±7.5°*

In the first case study (Case A.I), the main reflector of an OADE configuration was synthesized to radiate, under GO principles, a sectoral illumination in the elevation plane over ±7.5° with respect to the horizon (i.e., from $\theta_0 = 97.5°$ to $\theta_N = 82.5°$). As $\theta_0 > \theta_N$, the main reflector has a real caustic in the elevation plane (see Fig. 2). The subreflector generating ellipse was determined from a classical OADE configuration

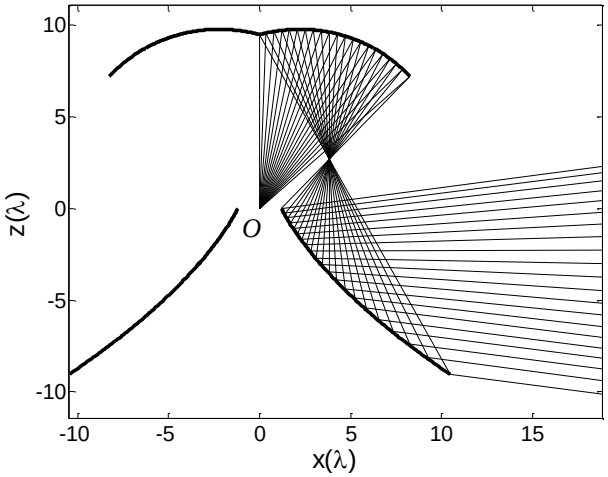

Fig. 3 – Generatrices of a shaped OADE dual-reflector antenna (Case A.II) with a virtual main-reflector caustic in the elevation plane.

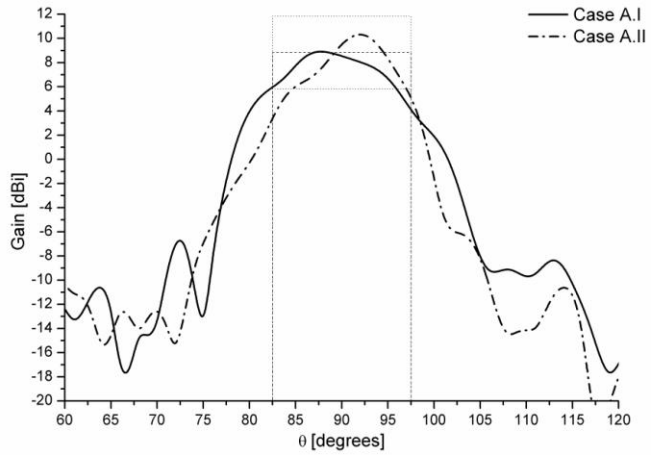

Fig. 4 – MoM radiation patterns (Cases A.I and A.II) in the elevation plane.

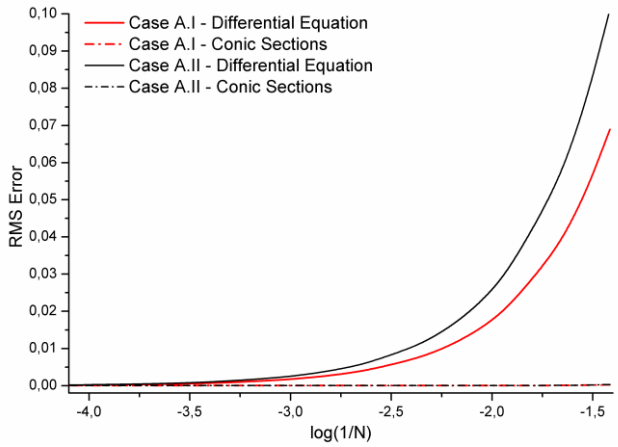

Fig. 5 – Main-reflector RMS error with respect to N for Cases A.I and A.II.

with the following parameters [8] (see Fig. 1): $V_S = 9.5\lambda$, $D_B = 2.4\lambda$, main-reflector projected diameter $D_M = 20\lambda$, focus O at the plane of the main-reflector central opening ($z_B = 0$), main-reflector aperture width $W_A = 8.25\lambda$, and $\gamma = 90°$. These values provide an ellipse with an eccentricity equal to 0.270899, an inter-focal distance $2c = 4.69\lambda$, and an axis with a tilt angle of 54.79° with respect to the z-axis. As a consequence, the projected diameter of the subreflector $D_S = 16.49\lambda$ and the subreflector edge angle $\theta_E = 48.72°$. These parameters also provide $r_{S0} = 3.77\lambda$ as an initial value for the shaping procedure presented in Sect. II. The generatrices of the subreflector and shaped main reflector are illustrated in Fig. 2.

In the second example (Case A.II), the subreflector is the same one used in Case A.I. The main reflector was shaped with an inverted far-field angular limits in the elevation plane (i.e., from $\theta_0 = 82.5°$ to $\theta_N = 97.5°$). As $\theta_N > \theta_0$, the main reflector now has a virtual caustic in the elevation plane (see Fig. 3). Some important dimensions of the shaped main reflector of Cases A.I and A.II are listed in Table I.

TABLE I

PARAMETERS	CASE A.I	CASE A.II	CASE B.I	CASE B.II
D_M (λ)	19.35	20.89	18.89	22.16
V_M (λ)	7.68	9.04	7.26	10.17
VOLUME($\lambda^3 10^3$)	4.2999	5.0105	4.1002	5.6606

From the table we observe that the projected main-reflector diameter D_M and height V_M of the real-caustic configuration (Case A.I) are smaller than those of the virtual-caustic configuration (Case A.II), indicating that the OADE configuration with a real-caustic main reflector occupies a smaller volume than its virtual-caustic counterpart.

The radiation patterns of Cases A.I and A.II were simulated by the method of moments (MoM) technique and are illustrated in Fig. 4, together with the prescribed GO far-field pattern of (12), used for the main-reflector shaping. As we can note, both results are close to the object function. The Differences observed can be attributed to diffractions effects and electromagnetic coupling not considered by the synthesis.

The shaping procedure discussed in Sect. II is simpler than those based on the evaluation of an ordinary differential equation, like that adopted in [2]. It also has a faster numerical convergence, providing the same precision of the procedure based on the solution of a differential equation with approximately 100 times less steps, as reported in [7]. To illustrate this feature, the main-reflector RMS error (with respect to a reflector shaped with a very large N value) obtained by the present technique and that of [2] are depicted in Fig. 5 as a function of log(1/N) for Cases A.I and A.II. The RMS behavior of both (real or virtual caustic) cases are basically the same and also the same of OADC axis-displaced configuration [7].

B. OADE Configuration for Sectoral Coverage over ±15°

The omnidirectional ADE configuration of Case B.I was designed to radiate, once again, a sectoral illumination in the elevation plane but over a wider range (±15° with respect to the horizon, (i.e., from $\theta_0 = 105°$ to $\theta_N = 75°$). The subreflector is the same of Cases A.I and A.II. The generatrices of the subreflector and shaped main reflector are illustrated in Fig. 6, where the real caustic of the main reflector is apparent. In last case study (Case B.II), the subreflector was kept the same of previous cases, and angular limits of far-field were inverted

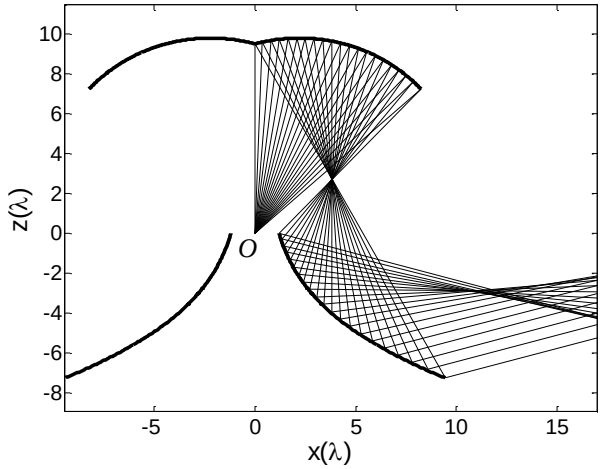

Fig. 6 – Generatrices of the shaped OADE dual-reflector antenna (Case B.I) with a real main-reflector caustic.

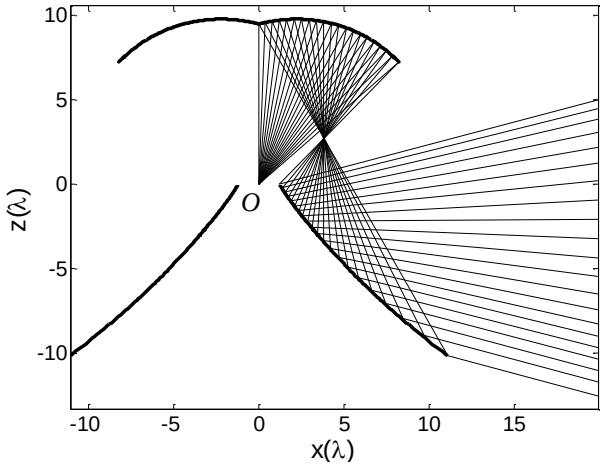

Fig. 7 – Generatrices of the shaped OADE dual-reflector antenna (Case B.II) with a virtual main-reflector caustic.

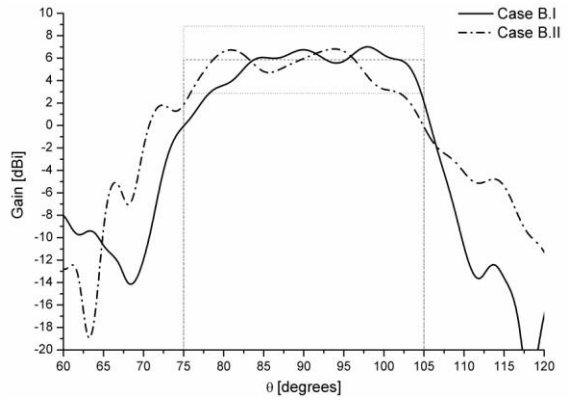

Fig. 8 – MoM radiation patterns (Cases B.I and B.II) in the elevation plane.

(i.e., from θ_0 = 75° to θ_N = 105°). As $\theta_N > \theta_0$, the main reflector now has a virtual caustic in the elevation plane (see Fig. 7). Once again, the antenna with a real main-reflector caustic presented a smaller volume, as can be inspected from Table I for Cases B.I and B.II. The radiation patterns of Cases B.I and B.II were simulated by the MoM and are illustrated in Fig. 8, together with the prescribed GO far-field pattern.

Comparing cases studies A and B we can note that when the desired sectoral illumination is attained for a wider angular range the radiation pattern is closer to the objective function than the in the narrower case. We can also observe (Fig. 8) that for Case B.I the gain moves further away from the objective region between θ = 75° and 80° and for Case B.II it occurs between θ = 100° and 105°. This happens because the subreflector has a lower illumination in regions close to θ_F = 0, as the feeder has a null radiation in this direction.

IV. CONCLUSIONS

This work presented an extension of the method for GO synthesis of the main reflector of OADE dual-reflector antennas. The procedure was demonstrated in the synthesis of four representative configurations, shaped to radiate a sectoral power density. For the cases investigated, the method has a numerical convergence higher than a traditional method based on the numerical integration of an ordinary differential equation. It was also observed that, the antennas with a real main-reflector caustic in the elevation plane have smaller dimensions than their virtual-caustic counterparts.

ACKNOWLEDGMENT

This work was made possible by support from, MCT/FINEP/CT/CNPq-554661/2010-1, and INCT Wireless Communications CNPq-573939/2008-0.

REFERENCES

[1] F. J. S. Moreira, A. Prata, Jr., and J. R. Bergmann, "GO Shaping of Omnidirectional Dual-Reflector Antennas for a Prescribed Equi-Phase Aperture Field Distribution," IEEE Transactions on Antennas and Propagation, vol. 55, no. 1, pp. 99—106, Jan. 2007.

[2] J. R. Bergmann and F. J. S. Moreira, "Omnidirectional ADE antenna with GO shaped main reflector for arbitrary far-field pattern in the elevation plane," IET Microwaves, Antennas & Propagation, vol. 3, no. 5, pp. 1028-1035, Oct. 2009.

[3] J. R. Bergmann and F. J. S. Moreira, "Bandwidth behavior of omnidirectional dual-reflector antennas synthesized for uniform coverage," Journal of Microwaves, Optoelectronics, and Electromagnetic Applications, vol. 8, no. 1, pp. S1—S8, June 2009.

[4] Y. Kim and T.-H. Lee, "Shaped circularly symmetric dual reflector antennas by combining local conventional dual reflector systems," IEEE Trans. Antennas Propagat. vol. 57, no 1, pp. 47-56, Jan. 2009.

[5] F. J. S. Moreira and J. R. Bergmann, "Shaping axis-symmetric dual-reflector antennas by combining conic sections," IEEE Trans. Antennas Propagat., vol. 59, no. 3, pp. 1042—1046, March 2011.

[6] F. J. S. Moreira and J. R. Bergmann, "Omnidirectional dual-reflector shaping by concatenating conic sections," 4th European Conf. Antennas and Propagation (EuCAP 2010), Barcelona, Spain, April 2010.

[7] R. A. Penchel, J. R. Bergmann, and F. J. S. Moreira, "An Omnidirectional Dual-Reflector Antenna with a Shaped Main Reflector Described by Local Conic Sections," 5th European Conference on Antennas and Propagation (EuCAP 2011), Rome, Italy, pp. 1221—1224, April 2011.

[8] F. J. S. Moreira and J. R. Bergmann, "Axis-Displaced Dual-Reflector Antennas for Omnidirectional Coverage with Arbitrary Main-Beam Direction in the Elevation Plane," IEEE Transactions on Antennas and Propagation, vol. 54, no. 10, pp. 2854—2861, Oct. 2006.

[9] B. S. Westcott, F. A. Stevens, and F. Brickell, "GO synthesis of offset dual reflectors," IEE Proc., Pt. H, vol. 128, no. 1, pp. 11–18, Feb. 1981.